Deep subwavelength plasmonic waveguide switch in double graphene layer structure

Hideo Iizuka and Shanhui Fan

Citation: Appl. Phys. Lett. **103**, 233107 (2013); doi: 10.1063/1.4839420
View online: http://dx.doi.org/10.1063/1.4839420
View Table of Contents: http://apl.aip.org/resource/1/APPLAB/v103/i23
Published by the AIP Publishing LLC.

Deep subwavelength plasmonic waveguide switch in double graphene layer structure

Hideo Iizuka[1,a)] and Shanhui Fan[2,b)]
[1]*Toyota Central Research and Development Labs, Nagakute, Aichi 480 1192, Japan*
[2]*Department of Electrical Engineering, Stanford University, Stanford, California 94305, USA*

(Received 8 October 2013; accepted 17 November 2013; published online 4 December 2013)

Graphene provides excellent prospects of the dynamic tunability, low propagation loss, and extreme mode confinement for plasmonic excitations in the infra-red and terahertz frequencies. We show that in a deep subwavelength double graphene layer structure, graphene plasmons can be routed between two different graphene waveguides by relatively small chemical potential tuning. We develop a coupled mode theory that completely accounts for the switching behavior observed in numerical simulations. Such a deep subwavelength 1×2 device is a crucial enabling component towards large-scale integrated deep-subwavelength electromagnetic circuits. © *2013 AIP Publishing LLC*. [http://dx.doi.org/10.1063/1.4839420]

In the fields of optics and electromagnetics, graphene[1,2] has generated substantial interests due to a number of its unique capabilities. As a single atomic layer material, graphene, nevertheless, interacts strongly with light at the near infra-red and visible wavelength range. Such an interaction moreover is tunable by varying the chemical potential. As a result, graphene has been widely explored to construct optical devices such as modulators[3,4] and detectors[5] and has been used to enable nonlinear optical interactions on chip.[6] These optical devices, however, typically have at least one of the dimensions beyond a single-wavelength.

In the longer wavelength range of 0.2 eV or less, graphene supports strong plasmonic response.[7–14] Graphene plasmons, with its tunability, enable active electromagnetic devices that are on the deep sub-wavelength scale. Several metamaterial-inspired concepts have been numerically demonstrated in graphene.[15] As a fundamental building block, graphene plasmonic waveguides have been numerically investigated.[16–18] Recent works have also developed concepts of sub-wavelength switches based on graphene plasmonics.[19,20] The switches in Refs. 19 and 20 however are based on tuning the absorption of a single graphene layer and functions only as a one-port modulator. As a further step, in this Letter, we present a design where graphene plasmons can be routed between two different graphene waveguides by relatively small chemical potential tuning. The overall device dimension is much smaller compared with the free-space wavelength of light. Such a 1×2 switch is a crucial enabling component for large-scale integrated electromagnetic circuits since it is the basic building block for complex switching and routing networks.

Figure 1(a) shows the configuration of a 1×2 waveguide switch for graphene plasmons. We assume a two-dimensional configuration. No electromagnetic field variation is assumed in the y-axis. The switch consists of the top and bottom graphene layers embedded in the three dielectric layers made of intrinsic or lightly doped silicon so that the top graphene layer can be biased by voltage V_g. The switch has a single input port on the bottom graphene layer (Port 1) and two output ports on the bottom (Port 2) and top (Port 3) graphene layers. The two graphene layers are parallel to each other within the finite length L along the x-axis. The distance between the two graphene layers increases beyond $x = L$.

We show that the structure in Fig. 1(a) behaves as a 1×2 switch when we vary the chemical potential of graphene. The optical conductivity σ of graphene consists of the Drude (intraband) and interband contributions and is related to the chemical potential μ through[21]

$$\sigma = \frac{i}{\omega + i/\tau}\frac{e^2 2k_bT}{\pi\hbar^2}\ln\left[2\cosh\frac{\mu}{2k_bT}\right] + \frac{e^2}{4\hbar}\left[G\left(\frac{\hbar\omega}{2}\right) + i\frac{4\hbar\omega}{\pi}\int_0^\infty \frac{G(\xi) - G(\hbar\omega/2)}{(\hbar\omega)^2 - 4\xi^2}d\xi\right], \quad (1)$$

where $G(\xi) = \sinh(\xi/k_bT)/[\cosh(\mu/k_bT) + \cosh(\xi/k_bT)]$. e, k_b, and $\hbar$ are the charge of an electron, the Boltzmann constant, and the reduced Planck constant, respectively. We assume an electron scattering lifetime $\tau = 0.5$ ps,[22–24] and a temperature of $T = 300$ K in Eq. (1). Near the frequency $\omega/(2\pi) = 30$ THz, such conductivity form indicates strong plasmonic response. Therefore changing the chemical potential allows one to change the propagation characteristics of graphene plasmons.

Using this form of graphene optical conductivity (Eq. (1)), we simulate the 1×2 switch with a simulator based on the finite integration technique.[25] Graphene is modeled as an equivalent dielectric material in simulation.[15] Graphene plasmon at a frequency of 30 THz is excited to propagate along the x-axis on the bottom layer and injected into Port 1. When $\mu_1 = \mu_2 = 0.6$ eV, we observe a complete transfer of the graphene plasmon to the top graphene layer at $x = L$ (Port 3) (Fig. 1(b)). However, when $\mu_1 = 0.6$ eV, $\mu_2 = 0.52$ eV, we observe a partial transfer of the graphene plasmon to the top layer around $x = L/2$. Moreover, at $x = L$ all the power is transferred back to the bottom layer and

a)hiizuka@mosk.tytlabs.co.jp
b)shanhui@stanford.edu

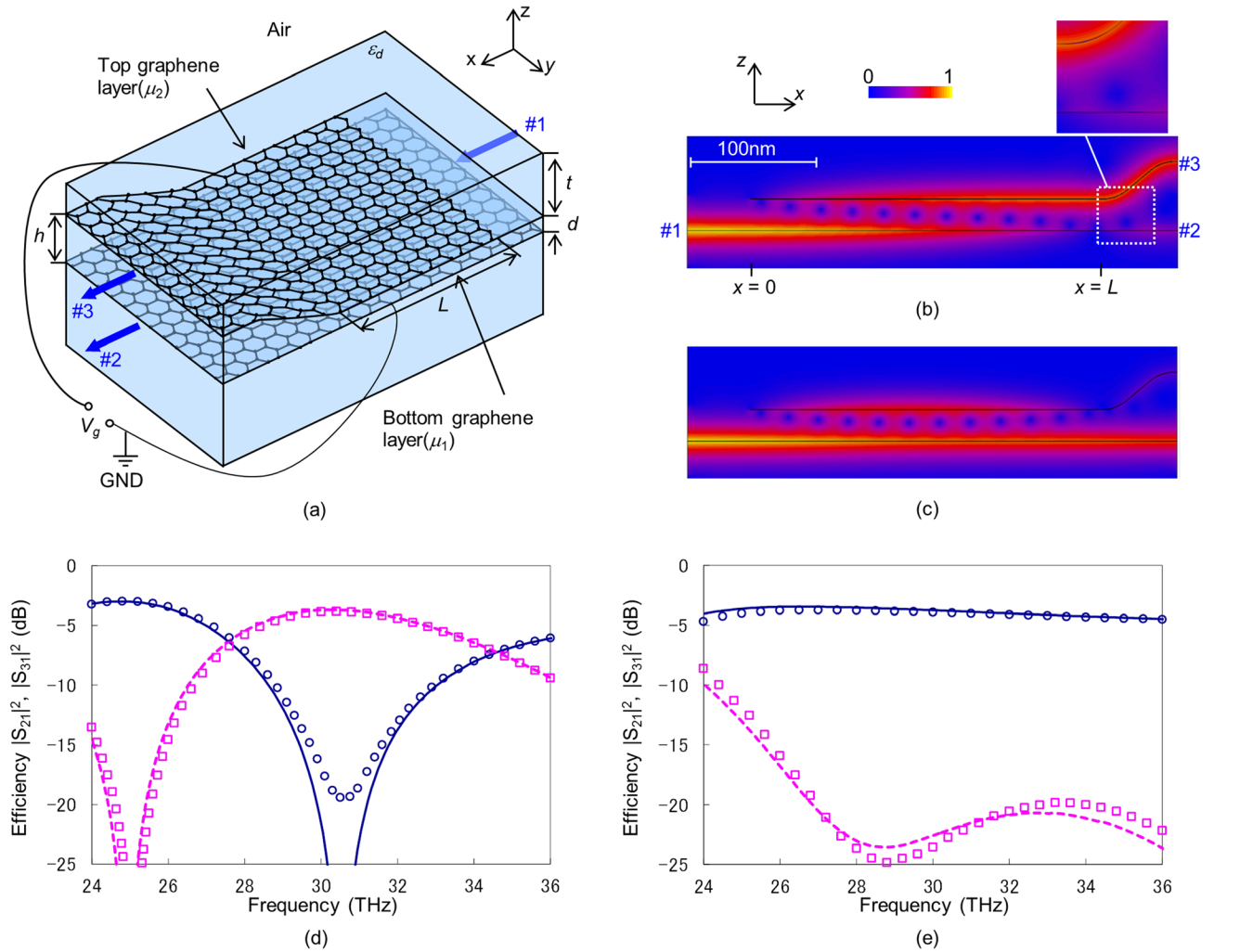

FIG. 1. 1×2 switch based on graphene plasmonics. (a) Configuration. It consists of the top and bottom graphene layers embedded in the three silicon layers. (b), (c) Snap shots of the electric field intensity $\sqrt{E_x^2 + E_z^2}$ distributions at 30 THz obtained by a simulator based on the finite-element-technique. (d), (e) Frequency responses of transmission ($|S_{21}|^2$) and transfer ($|S_{31}|^2$) efficiencies. The bottom and top graphene layers have the same chemical potential of $\mu_1 = \mu_2 = 0.6\,\text{eV}$ for (b), (d) and different values of $\mu_1 = 0.6\,\text{eV}$, $\mu_2 = 0.52\,\text{eV}$ for (c), (e). Curves are obtained by the coupled mode theory, and symbols are numerical results of the simulation in (d), (e) (blue solid lines and circles, $|S_{21}|^2$; pink dashed lines and squares, $|S_{31}|^2$). ($L = 280\,\text{nm}$, $t = 70\,\text{nm}$, $d = 25\,\text{nm}$, $h = 55\,\text{nm}$, $\varepsilon_d = 14$).

output through Port 2 (Fig. 1(c)). A modest change of chemical potential therefore allows us to switch the output between the two waveguides. The length of the switch is $L = 280\,\text{nm}$ whereas the spacing between the graphene layers is 25 nm. We therefore have a deep subwavelength device.

In Figs. 1(d) and 1(e) we plot as dots the simulated spectra of transmission efficiency ($|S_{21}|^2$) and the transfer efficiency ($|S_{31}|^2$) for the two sets of chemical potentials. As indicated above, for $\mu_1 = \mu_2 = 0.6\,\text{eV}$ (Fig. 1(d)), we have a strong transfer (i.e., large $|S_{31}|^2$) at the frequency of 30 THz. The ratio of the power of $|S_{31}|^2$ to $|S_{21}|^2$ is larger than 10 dB over a frequency bandwidth of 2.1 THz (7%), indicating a relatively broadband frequency response. We note that the frequency where peak transfer occurs is related to the choice of L, and a different choice of L can be used to accomplish high transfer efficiency at other frequencies. On the other hand, when $\mu_1 = 0.6\,\text{eV}$, $\mu_2 = 0.52\,\text{eV}$, we observe very little transfer (i.e., very small $|S_{31}|^2$) over the entire frequency range of 24–36 THz where we did the calculation. The transmission shows an overall loss of 5 dB over the same frequency range, indicating a relatively low loss device.

We now develop an analytic model to account for the numerical results in Fig. 1. This model will also be used to highlight some of the design considerations for this kind of switch. Figure 2 shows the analytic model. a_1 and a_2 are the wave amplitudes of the graphene plasmon modes on the bottom and top graphene layers, respectively. These amplitudes are normalized so that the power in each mode is $|a_1|^2$ and $|a_2|^2$, respectively. We assume that the plasmon modes of each layer, when these layers are uncoupled, have

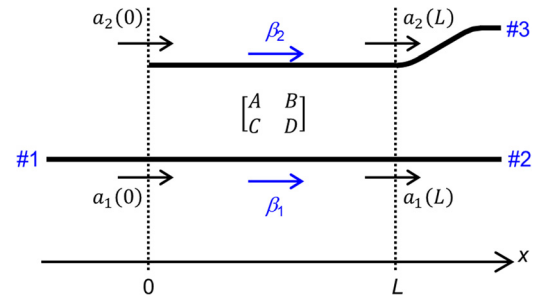

FIG. 2. Analytic model of the 1×2 switch in Fig. 1(a).

wavenumbers β_1 and β_2. When the two layers are coupled, the coupling constants between the two layers are κ_{12} and κ_{21}. The energy conservation constrains the coupling constants $\kappa_{12} = \kappa_{21}^*$. Assuming that the two graphene layers are weakly coupled, i.e., $|\kappa_{12}| \ll |\beta_1|, |\beta_2|$, the graphene plasmon waves propagating in the forward direction are characterized at $x = 0, L$ by[26]

$$\begin{bmatrix} a_1(L) \\ a_2(L) \end{bmatrix} = \begin{bmatrix} A & B \\ C & D \end{bmatrix} \begin{bmatrix} a_1(0) \\ a_2(0) \end{bmatrix}, \tag{2a}$$

where

$$A = \cos(\beta_0 L) + i\left[(\beta_2 - \beta_1)/(2\beta_0)\right]\sin(\beta_0 L), \tag{2b}$$

$$B = (\kappa_{12}/\beta_0)\sin(\beta_0 L), \tag{2c}$$

$$C = (\kappa_{21}/\beta_0)\sin(\beta_0 L), \tag{2d}$$

$$D = \cos(\beta_0 L) + i\left[(\beta_1 - \beta_2)/(2\beta_0)\right]\sin(\beta_0 L), \tag{2e}$$

$$\beta_0 = \sqrt{\left[(\beta_1 - \beta_2)/2\right]^2 + |\kappa_{12}|^2}. \tag{2f}$$

Substituting $a_2(0) = 0$ into Eq. (2a), we obtain the transmission and transfer efficiencies

$$|S_{21}|^2 = |a_1(L)/a_1(0)|^2 = |A|^2, \tag{3a}$$

$$|S_{31}|^2 = |a_2(L)/a_1(0)|^2 = |C|^2. \tag{3b}$$

From the theory above, complete transfer between the two waveguides can be achieved when $\beta_1 = \beta_2$ and $\kappa_{12} L = \pi/2$ for the smallest L whereas zero-transfer between the two waveguides can be achieved when $\beta_1 \neq \beta_2$ and $\beta_0 L = \pi$; the coupling length for $\beta_1 \neq \beta_2$ is half of that for $\beta_1 = \beta_2$. We therefore see that tuning the dispersion relation of a single sheet, e.g., by changing β_1, is sufficient to achieve routing of graphene plasmons between the two waveguides. Also, to achieve complete transfer, the phase matching between the two waveguides (i.e., $\beta_1 = \beta_2$ at the operating frequency) is important. Therefore, in our design, the use of top silicon region is important as it facilitates the phase-matching between the plasmons on the two sheets.

The parameters in the coupled mode theory above, i.e., $\beta_{1,2}$ and κ_{12}, can be determined by analytic calculation of the dispersion relation of graphene plasmons in the double layer structure. When the top dielectric substrate has enough thickness to be assumed infinite, the dispersion equation for the double graphene layer structure is given by[20]

$$\left(2\frac{\varepsilon_d}{\kappa_d} + i\frac{\sigma_1}{\omega\varepsilon_0}\right)\left(2\frac{\varepsilon_d}{\kappa_d} + i\frac{\sigma_2}{\omega\varepsilon_0}\right)\exp(\kappa_d d) + \frac{\sigma_1\sigma_2}{(\omega\varepsilon_0)^2}\exp(-\kappa_d d) = 0, \tag{4}$$

where $\kappa_d = \sqrt{\beta^2 - \varepsilon_d k_0^2}$, $\left(\beta^2 > \varepsilon_d k_0^2\right)$. ε_0 is the permittivity of free space. Two wavenumbers β_c for the common mode and β_d for the differential mode in the double graphene layer structure are calculated using Eq. (4). On the two graphene layers, the common or differential modes have the x-direction electric fields with the same or opposite signs, respectively. When the two layers are uncoupled, the wavenumber β_1 (β_2) for the bottom (top) graphene layer is obtained by[8]

$$2\frac{\varepsilon_d}{\kappa_d} + i\frac{\sigma_{1,2}}{\omega\varepsilon_0} = 0. \tag{5}$$

The coupling constant κ_{12} between the top and the bottom graphene layers can be obtained by using the coupled mode theory to relate the dispersion relations of Eqs. (4) and (5)

$$\begin{bmatrix} -i\beta_1 & \kappa_{12} \\ \kappa_{21} & -i\beta_2 \end{bmatrix} = \boldsymbol{M}\begin{bmatrix} -i\beta_d & 0 \\ 0 & -i\beta_c \end{bmatrix}\boldsymbol{M}\ , \tag{6a}$$

where

$$\boldsymbol{M} = \begin{bmatrix} -i\left[(\beta_1 - \beta_2)/2 + \beta_0\right] & \kappa_{12} \\ \kappa_{21} & i\left[(\beta_1 - \beta_2)/2 + \beta_0\right] \end{bmatrix}. \tag{6b}$$

Using Eqs. (6a) and (6b), κ_{12} is expressed with the four wavenumbers

$$|\kappa_{12}| = (1/2)\sqrt{(\beta_d - \beta_c)^2 - (\beta_1 - \beta_2)^2}. \tag{7}$$

We use the theory above to understand the behavior of the 1×2 switch. We start by comparing the analytic dispersion relations described above with numerical calculations of the eigenmodes. Figures 3(a) and 3(b) show the simulated magnetic field H_y distributions of the common and differential modes at a frequency of 30 THz when $\mu_1 = \mu_2 = 0.6$ eV. Observe that the magnetic fields are extremely confined on the graphene layers. The wavelengths λ_g of both modes are approximately 50 nm (0.005 λ_0) and are far smaller than the corresponding free-space wavelength. The common (Fig. 3(a)) and differential modes (Fig. 3(b)) have the out-of-phase and in-phase distributions in the y component of the magnetic field, respectively, in the interlayer along the z direction. Numerical results (blue circle and pink square in Fig. 3(c)) for the dispersion relation of the common and differential modes agree well with the analytic results calculated using Eq. (4) (blue solid line and pink dashed dotted line in Fig. 3(c)). The dispersion curve (green dashed line) of the single graphene layer with a chemical potential of 0.6 eV is also presented in Fig. 3(c). It lies between the dispersion curves of the common and differential modes as expected from the analytic theory.

Figs. 3(d)–3(f) show the behaviors of the modes when the two graphene layers have different chemical potentials $\mu_1 = 0.6$ eV, $\mu_2 = 0.52$ eV. Unlike the equal chemical potential case above, where both the common and the differential modes have equal field strength in the two graphene layers, here the common mode is mostly concentrated on the bottom graphene layer (Fig. 3(d)), and the differential mode is mostly concentrated on the top layer (Fig. 3(e)). At large wavenumbers, the dispersion relations of the common and differential modes approach those of individual graphene layers at $\mu_1 = 0.6$ eV, $\mu_2 = 0.52$ eV, respectively (Fig. 3(f)).

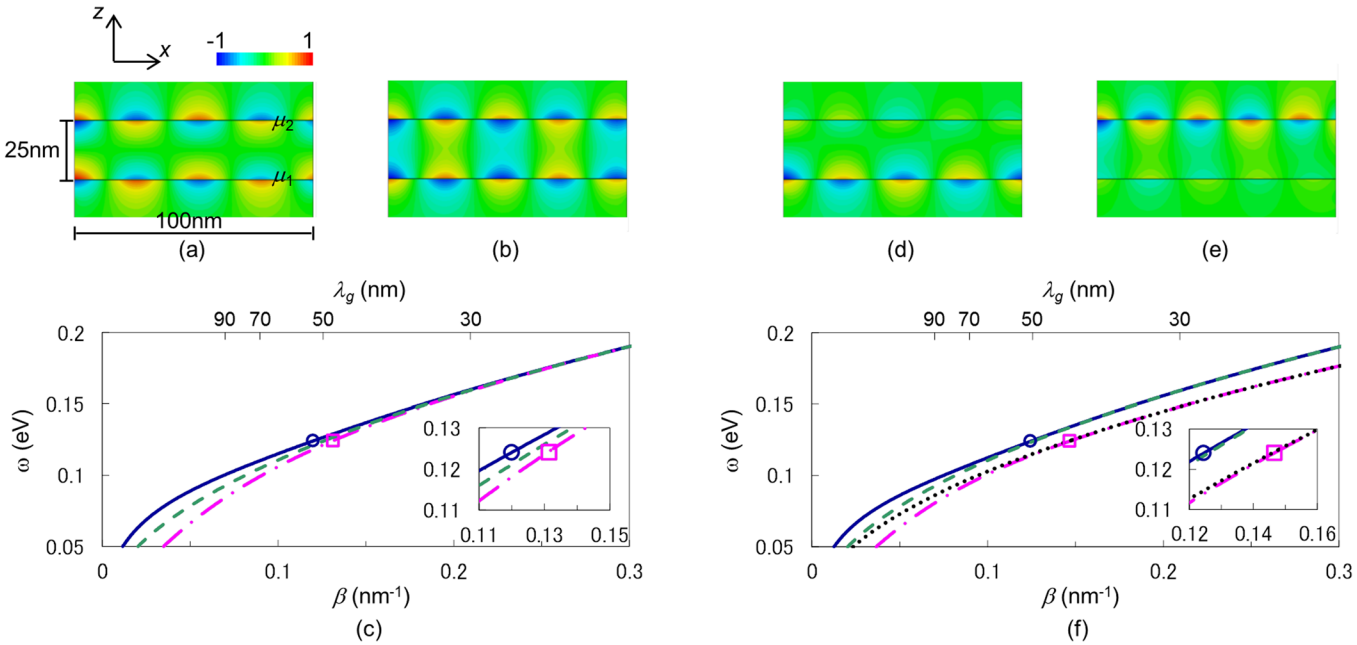

FIG. 3. Snap shots of the magnetic field H_y distributions of (a), (d) the common mode and (b), (e) the differential mode at 30 THz, and (c), (f) dispersion curves in the double graphene layer structure. Chemical potentials are set at $\mu_1 = \mu_2 = 0.6$ eV for (a)–(c) and $\mu_1 = 0.6$ eV, $\mu_2 = 0.52$ eV for (d)–(f). Magnetic field distributions of (a), (b), (d), and (e) and symbols in (c), (f) are numerical results of the finite integration technique based simulation. Curves in (c), (f) are obtained using Eq. (4) (blue solid lines and circles, β_c; pink dotted-dashed lines and squares, β_d). Dispersion curves of a single graphene layer with chemical potentials of 0.6 eV (green dashed lines) and 0.52 eV (black dotted line) are also presented using Eq. (5) ($d = 25$ nm, $\varepsilon_d = 14$).

The modal behaviors as discussed above underlie the switching effect. When the chemical potential of the graphene layers matches, both common and differential modes have equal field intensity in the two layers. An incident wave exciting one of the graphene layers results in a linear superposition of the common and differential modes and hence power transfers between the layers. On the other hand, when the two layers have different chemical potentials, the transfer is suppressed since the eigenmodes are predominantly in either one of the layers.

Using the analytically determined dispersion relation as parameters, we apply Eqs. (2) and (3) to solve for the parameters S_{21}, S_{31} of the 1×2 switch and compare to numerical simulations (Figs. 1(d) and 1(e)). The analytical results agree excellently with numerical results. At 30 THz, the analytic results show a coupling constant of $|\kappa_{12}/\beta_0| = 1$ for $\mu_1 = \mu_2 = 0.6$ eV and $|\kappa_{12}/\beta_0| = 0.43$ for $\mu_1 = 0.6$ eV, $\mu_2 = 0.52$ eV, which correspond to the cases of complete (Fig. 1(b)) and near-zero transfers (Fig. 1(c)) between the two graphene layers, respectively. The discrepancy between the analytic and numerical results around the frequency of 30THz comes from the weak but non-vanishing coupling from the curved top layer to the bottom layer, as shown in the inset of Fig. 1(b). To account for such a coupling, we choose an effective coupling length of $L = 310$ nm in Eqs. (2) and (3); a length that is longer than the length of the parallel regions at 280 nm.

The overall dimension of this 1×2 switch is much smaller compared with conventional photonic switches, including switches based on silicon waveguides or photonic crystals. The device here is far more compact because it exploits unique properties of graphene, including the deep-subwavelength confinement properties of graphene plasmons, and the ability to tune graphene plasmons by modest voltage change. The waveguide 1×2 switch is a fundamental building block for large-scale integration of electromagnetic circuits. For example, it has been emphasized recently that any linear optical functionalities can be realized by cascading such waveguide switches.[27]

A double graphene layer modulator has been experimentally demonstrated,[4] and the structure of Fig. 1 may be fabricated by current nanofabrication technology similar to Ref. 4. Regarding the tolerance of the device, we note that the switch behavior is sensitive to the distance between the graphene layers and their chemical potentials. For example, the dispersion analysis estimates that the coupling length changes from 200 nm to 420 nm for a ± 3 nm variation of the interlayer thickness and from 240 nm to 350 nm for a ± 0.05 eV variation of chemical potentials of graphenes. For each interlayer thickness considered here, one can always choose an appropriate voltage to achieve switching and the performance of the device is therefore robust.

In conclusion, we have shown that the unique electromagnetic properties of graphene enable the construction of a fundamentally important building block of large-scale integrated electromagnetic circuit at deep sub-wavelength scales.

The authors would like to thank Dr. Yasuhiko Takeda for useful comments on graphene characteristics. Professor Fan's contribution to this publication was as a consultant, and was not part of his Stanford duties or responsibilities.

[1]K. S. Novoselov, A. K. Geim, S. V. Morozov, D. Jiang, Y. Zhang, S. V. Dubonos, I. V. Grigorieva, and A. A. Firsov, Science **306**, 666 (2004).
[2]Y. Zhang, Y. W. Tan, H. L. Stormer, and P. Kim, Nature **438**, 201 (2005).
[3]M. Liu, X. Yin, E. Ulin-Avila, B. Geng, T. Zentgraf, L. Ju, F. Wang, and X. Zhang, Nature **474**, 64 (2011).
[4]M. Liu, X. Yin, and X. Zhang, Nano Lett. **12**, 1482 (2012).
[5]T. Mueller, F. Xia, and P. Avouris, Nat. Photonics **4**, 297 (2010).

[6]T. Gu, N. Petrone, J. F. McMillan, A. van der Zande, M. Yu, G. Q. Lo, D. L. Kwong, J. Hone, and C. W. Wong, Nat. Photonics **6**, 554 (2012).
[7]A. N. Grigorenko, M. Polini, and K. S. Novoselov, Nat. Photonics **6**, 749–758 (2012).
[8]M. Jablan, H. Buljan, and M. Soljacic, Phys. Rev. B **80**, 245435 (2009).
[9]S. A. Mikhailov and K. Ziegler, Phys. Rev. Lett. **99**, 016803 (2007).
[10]E. H. Hwang and S. D. Sarma, Phys. Rev. B **75**, 205418 (2007).
[11]F. H. L. Koppens, D. E. Chang, and F. J. Garcia de Abajo, Nano Lett. **11**, 3370 (2011).
[12]L. Ju, B. Geng, J. Horng, C. Girit, M. Martin, Z. Hao, H. A. Bechtel, X. Liang, A. Zettl, Y. R. Shen, and F. Wang, Nat. Nanotechnol. **6**, 630–634 (2011).
[13]H. Yan, X. Li, B. Chandra, G. Tulevski, Y. Wu, M. Freitag, W. Zhu, P. Avouris, and F. Xia, Nat. Nanotechnol. **7**, 330 (2012).
[14]H. Yan, T. Low, W. Zhu, Y. Wu, M. Freitag, X. Li, F. Guinea, P. Avouris, and F. Xia, Nat. Photonics **7**, 394 (2013).
[15]A. Vakil and N. Engheta, Science **332**, 1291 (2011).
[16]J. Christensen, A. Manjavacas, S. Thongrattanasiri, F. H. L. Koppens, and F. J. G. de Abajo, ACS Nano **6**, 431 (2012).
[17]A. Y. Nikitin, F. Guinea, F. J. Garcia-Vidal, and L. Martin-Moreno, Phys. Rev. B **84**, 161407(R) (2011).
[18]X. Zhu, W. Yan, N. A. Mortensen, and S. Xiao, Opt. Express **21**, 3486 (2013).
[19]J. S. Gomez-Diaz and J. Perruisseau-Carrier, Opt. Express **21**, 15490 (2013).
[20]D. Svintsov, V. Vyurkov, V. Ryzhii, and T. Otsuji, J. Appl. Phys. **113**, 053701 (2013).
[21]L. Falkovsky, J. Phys. Conf. Ser. **129**, 012004 (2008).
[22]K. I. Bolotin, K. J. Sikes, Z. Jiang, M. Klima, G. Fudenberg, J. Hone, P. Kim, and H. L. Stormer, Solid State Commun. **146**, 351 (2008).
[23]D. Mann, A. Javey, J. Kong, Q. Wang, and H. Dai, Nano Lett. **3**, 1541 (2003).
[24]P. Li and T. Taubner, ACS Nano **6**, 10107 (2012).
[25]See http://www.cst.com for CST Microwave Studio, 2012.
[26]H. A. Haus, *Waves and Fields in Optoelectronics* (Prentice-Hall, Englewood Cliffs, NJ, 1984).
[27]D. A. Miller, Opt. Express **20**, 23985 (2012).